

Geophysical Research Letters

RESEARCH LETTER

10.1029/2020GL090123

Key Points:

- An irrigated turf grass exhibits the oasis effect on the energy balance during 36% of warm season days, including excessive heat warnings
- During oasis days, advected energy from surrounding urban areas enhances evaporative cooling, which arises from abiotic mechanisms
- A new method to identify oasis days using daily air temperature and relative humidity can be applied to urban parks in desert regions

Supporting Information:

- Supporting Information S1

Correspondence to:

E. R. Vivoni,
vivoni@asu.edu

Citation:

Vivoni, E. R., Kindler, M., Wang, Z., & Pérez-Ruiz, E. R. (2020). Abiotic mechanisms drive enhanced evaporative losses under urban oasis conditions. *Geophysical Research Letters*, 47, e2020GL090123. <https://doi.org/10.1029/2020GL090123>

Received 4 AUG 2020



Accepted 4 NOV 2020

Accepted article online 16 NOV 2020

©2020. The Authors.

This is an open access article under the terms of the Creative Commons Attribution License, which permits use, distribution and reproduction in any medium, provided the original work is properly cited.

Abiotic Mechanisms Drive Enhanced Evaporative Losses under Urban Oasis Conditions

Enrique R. Vivoni^{1,2} , Mercedes Kindler² , Zhaocheng Wang² , and Eli R. Pérez-Ruiz^{1,3} 

¹School of Earth and Space Exploration, Arizona State University, Tempe, AZ, USA, ²School of Sustainable Engineering and the Built Environment, Arizona State University, Tempe, AZ, USA, ³Departamento de Ingeniería Civil y Ambiental, Universidad Autónoma de Ciudad Juárez, Ciudad Juárez, Mexico

Abstract The oasis effect refers to the impact of advected energy on the surface energy balance leading to enhanced evapotranspiration. In this study, we utilize a 1-yr record of water, energy, and carbon dioxide (CO₂) fluxes to study the occurrence and signature of the oasis effect in an irrigated turf grass of an arid urban region. Days with the oasis effect are selected using readily available air temperature and relative humidity and include excessive heat warnings. During oasis days, higher evaporative cooling is demonstrated throughout the day, especially for late afternoons when it can exceed net radiation. Evaporative enhancements are linked to abiotic mechanisms, such as soil and irrigation water evaporation, since plant productivity is unaltered. Nighttime evaporative losses and CO₂ releases are also enhanced during oasis days. Our findings show how the oasis effect impacts the water, carbon, and thermal conditions of urban parks.

1. Introduction

Irrigation allows the maintenance of vegetation which supports evaporative cooling, significantly reducing air and surface temperatures and enhancing atmospheric water content (e.g., Gober et al., 2010; Myint et al., 2013; Song & Wang, 2015). Sharp thermal and moisture contrasts are often created between irrigated areas and their surrounding landscapes (Chow et al., 2012; Ko et al., 2016). An example of this is the establishment of irrigated turf grasses in urban parks and golf courses which are surrounded by land cover types with less or no irrigation. These sharp contrasts in irrigation have the potential for creating an “oasis effect” whereby advected energy from hotter and drier surrounding areas from all directions can influence the irrigated site (Warner, 2004). A separate impact of irrigated sites on downwind areas is also expected (e.g., Motazedian et al., 2020). Identifying the presence of the oasis effect and the mechanisms leading to its consequences on the surface energy balance is critical in urban parks of arid and semiarid regions since these provide ecosystem services related to heat amelioration (Harlan et al., 2006), biodiversity (Cook & Faeth, 2006), cultural amenities (Park, 2017), aesthetics (Yabiku et al., 2008), and real estate prices (Larson & Perrings, 2013).

Continuous, in situ measurements of the surface energy balance in urban parks are generally lacking, thus limiting our understanding of the effects of irrigation on water, energy, and carbon dioxide (CO₂) fluxes. Most prior studies are limited to short periods that do not capture the strong seasonal variations that often exist in radiative forcing, outdoor water use, and turf grass management (e.g., Chow et al., 2011; Colter et al., 2019; Day et al., 2002; Pérez-Ruiz et al., 2020; Sproken-Smith et al., 2000; Templeton et al., 2018). In addition, the atmospheric conditions leading to the oasis effect are not well understood, in particular whether or not readily available data are sufficient for its identification. It is also unclear if a direct relationship exists with excessive heat warnings (EHWs) during which these sites serve as thermal refugia (e.g., Brown et al., 2015). Since urban parks and golf courses often occupy large surface areas in arid and semiarid regions, it is possible that their interactions with the atmosphere can also have regional consequences on the urban heat island (Buyantuyev & Wu, 2010), the CO₂ dome (Koerner & Klopatek, 2002), and the precipitation regime (Shepherd, 2006), among others.

In this study, we address this knowledge gap through the use of the eddy covariance (EC) method to measure water, energy, and CO₂ fluxes at an irrigated urban park in a desert region. EC measurements provide high-temporal resolution data that are useful for quantifying turbulent fluxes and identifying linkages

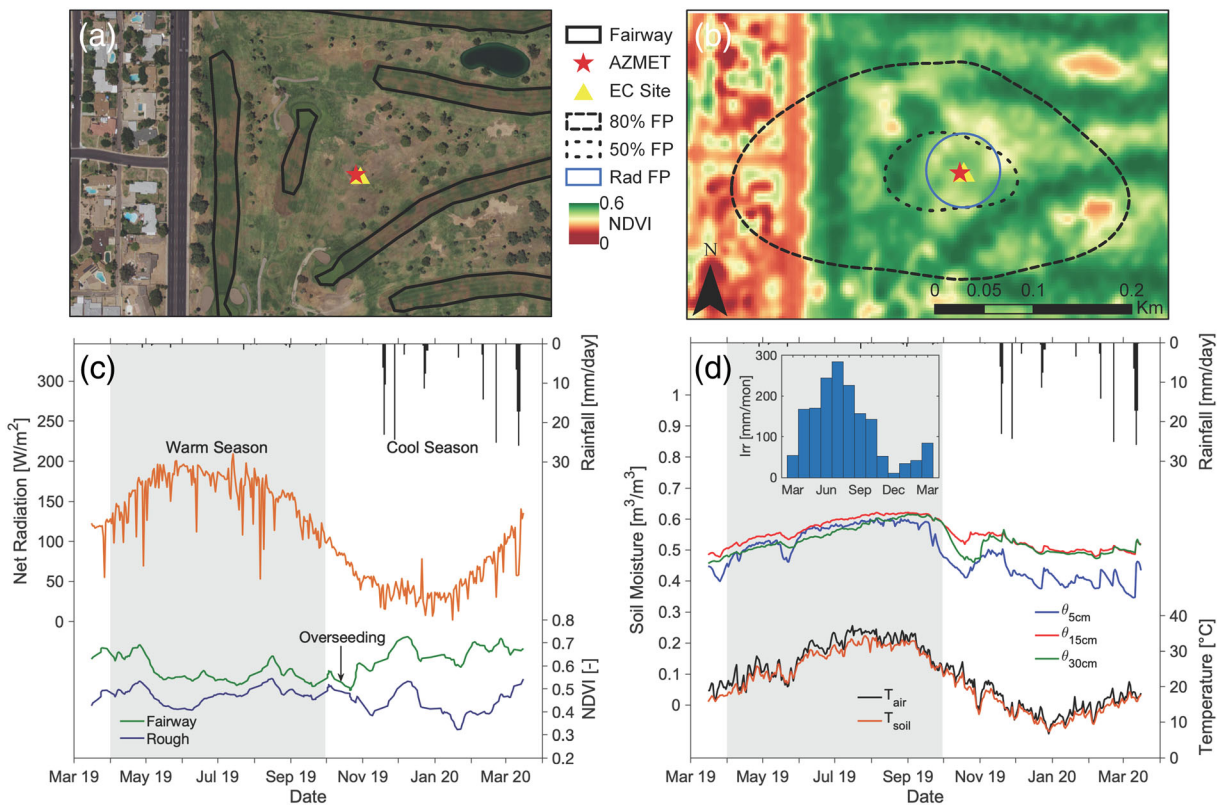


Figure 1. (a) Encanto Golf Course in Phoenix, AZ, with location of EC site and AZMET station. (b) Spatial distribution of *NDVI* at 3-m resolution with the EC footprint (FP) estimated at 50% and 80% contributions, each averaged over the warm season, and radiometer footprint (Rad FP). (c, d) Daily variations in rainfall, net radiation, *NDVI* for fairway and rough areas, soil moisture at three depths, and air and soil temperature during the warm and cool seasons. Inset in (d) shows monthly estimates of irrigation at Encanto Golf Course.

between them that reveal the role played by urban ecosystems (e.g., Baldocchi et al., 2001). The study period allows investigating seasons when irrigation and turf grass management vary considerably, including EHW periods during the North American monsoon (see <http://www.weather.gov/psr/HeatSafety>). Through ancillary measurements, we aim to understand how the surface energy balance is altered under the oasis effect due to the omnidirectional effects of neighboring urban sites on the golf course. In particular, we address if changes in evapotranspiration driven by the oasis effect are linked to abiotic or biotic mechanisms through an analysis of coincident CO₂ fluxes. van Bavel et al. (1963) argued that enhanced plant transpiration explained these changes but did not benefit from simultaneous water, energy, and CO₂ fluxes for exploring the underlying mechanisms.

2. Methods

2.1. Study Location

The study site is located in the northwest corner of the 18-hole Encanto Golf Course in Phoenix, Arizona, USA (33.48°N, -112.10°W, 334 m; Figure 1a). At the site, the Arizona Meteorological Network (AZMET; <https://cals.arizona.edu/AZMET/>) placed a weather station in 1988 to estimate reference evapotranspiration. We installed additional sensors inside the fenced area of the AZMET station over the period 16 March 2019 to 16 March 2020. Turf management at Encanto Golf Course includes varying treatments in fairways and rough areas, using warm season bermudagrass (*Cynodon dactylon*) and overseeding with ryegrass (*Lolium perenne*) to maintain grass cover during the cool season. Soils at the site are well-drained Mohall clay loam that have undergone several decades of soil and water treatments (Soil Survey Staff, 2020). While turf grass is nearly continuous in cover, a few scattered palms are found in rough areas and trees line nearby streets (170 m to west of EC site). The site is immersed in a low-density urban fabric consisting of

single-family residences, commercial areas, streets, and parking lots. Local climate is classified as hot and arid (Köppen zone BWh) with an average annual rainfall of 203 mm/yr (AZMET data over the period 1989–2019), with small differences between warm (87 mm, 1 April to 30 September) and cool (116 mm, 1 October to 31 March) seasons. Similar conditions are expected in other urban parks and golf courses that occupy about 32 km² or 2.4% of the City of Phoenix area.

2.2. Surface Energy Balance Measurements

The EC method consists of an open path-infrared gas analyzer to measure H₂O and CO₂ concentrations (LI-7500A, Li-COR Biosciences) and a three-dimensional sonic anemometer (CSAT-3, Campbell Scientific) to measure turbulent wind velocities. The EC system was installed at 5 m above the ground and aligned with the dominant wind direction (180° from North) to measure latent heat flux (λET), sensible heat flux (H), and net ecosystem exchange (NEE). A radiometer (CNR4, Kipp & Zonen) was installed at a 4 m height to measure net radiation (R_n), while a heat flux plate (HFP01SC, Hukseflux) was buried at 5 cm depth to estimate ground heat flux (G). Sensor placement and measurement heights were selected to sample turf grass conditions in a small EC footprint obtained using the two-dimensional model of Kljun et al. (2015) at the daily scale and aggregated for each season. Figure 1b illustrates the 50% and 80% source areas during the warm season. Vegetation within the 50% and 80% footprints were classified as grass (98% and 81%), tree (2% and 8%), bare soil (<1% and 4%), and impervious surface (0% and <8%), respectively, based on a 1-m land cover classification obtained in 2010 (Li et al., 2014). Fluxes were calculated at 30-min intervals with EddyPro[®] 7.0.4. EC processing included a number of standard processing steps (supporting information Text S1). Missing data accounted for 21% of the study period due to maintenance and power issues. The energy balance yielded that 90% of available energy ($R_n - G$) was measured as turbulent fluxes ($\lambda ET + H$), consistent with studies in different ecosystems (Wilson et al., 2002; see Figure S1).

2.3. Ancillary Data Sets

Ancillary measurements were installed to complement the AZMET records, including: (1) volumetric soil moisture at 5-, 15-, and 30-cm depths (θ , CS616, Campbell Sci.), (2) soil temperature at 2- and 6-cm depths (TCAV-L, Campbell Sci., averaged as T_{soil}), (3) land surface temperature (LST) estimated from longwave radiation, following Martin et al. (2019), and (4) midday albedo (a) obtained from the radiometer. We used AZMET data for rainfall (R), air temperature (T_{air}), vapor pressure deficit (VPD), relative humidity (RH), incoming solar radiation (R_s), wind speed and direction, and reference evapotranspiration (ET_o). Monthly estimates of water use via sprinkler irrigation were provided by the City of Phoenix based on metering. In addition, we used high spatiotemporal resolution data on the normalized difference vegetation index ($NDVI$) from Planet Labs (2017), to quantify turf grass conditions. PlanetScope products (3 m, daily resolution; Text S2) were obtained from a constellation of >130 active Cubesats in four spectral bands. A total of 201 cloud-free scenes (54.6% of study period) at an overpass time from 9:30 to 11:30 a.m. were converted into a linearly interpolated $NDVI$ series (Chen et al., 2004). Bias correction was then used to adjust $NDVI$ to match coincident values obtained from Landsat 8. PlanetScope has been applied in agricultural areas (Houborg & McCabe, 2018), but its observing capabilities in urban parks and golf courses have not been demonstrated.

3. Results and Discussion

3.1. Seasonal Variations

Figures 1c and 1d display the annual cycle in soil, vegetation, and meteorological variables during the study period. These were selected to show the water and energy input and the resulting soil and turf grass conditions in the warm and cool seasons. Net radiation (R_n) tracks the seasonal variation in solar irradiance and daily changes linked to rainfall and cloud cover. During the warm season, rainfall (R) was below average, while air temperature (T_{air}) was above average (8 mm and 29.2°C as compared to 87 mm and 28.8°C from 1989 to 2019), consistent with analyses indicating exceptionally hot and dry conditions (National Weather Service [NWS], 2019). This included 26 days of EHWs between 11 June to 7 September 2019. During the cool season, R was above average (177% of 1989–2019 average), including 4 days with $R > 20$ mm/day, which has a low probability (<2%; Mascaro, 2018). When compared to irrigation (Figure 1d inset), however, R is a negligible to minor input for the warm and cool seasons (<1% and 36% of total, respectively). Based on turf guidance (Brown et al., 2001), sprinkler irrigation occurs daily in the warm season in the entire golf course,

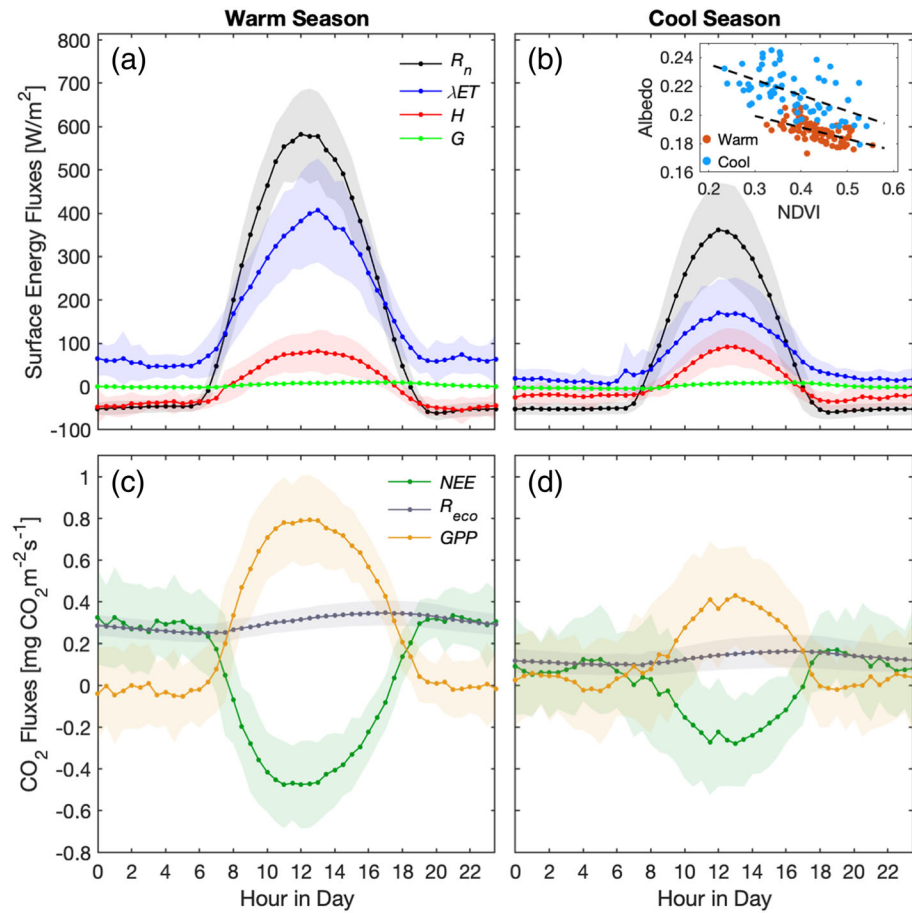


Figure 2. Diurnal cycles of (a, b) surface energy fluxes and (c, d) CO₂ fluxes during the warm and cool seasons. Symbols indicate average values for each 30-min interval in each season, while envelopes depict the ± 1 standard deviation. Inset in (b) shows the daily relations between midday albedo and NDVI for the warm and cool seasons, including linear regressions (see Text S3).

whereas only fairways receive daily irrigation during the cool season and roughs are irrigated once per week. Irrigation increases soil moisture (θ) during the warm season down to 30-cm depth (Figure 1d), which sustains high NDVI (Figure 1c). Decreases in irrigation in the cool season are reflected in lower θ and decreases in NDVI in rough areas, whereas overseeding and irrigation in fairways promotes continued NDVI (see Text S2 and Figure S2).

In addition to wet soil conditions, frequent irrigation promotes evaporative cooling which impacts the relation between daily T_{air} and T_{soil} (Figure 1d). A lower T_{soil} was noted in the turf grass for the warm season as compared to T_{air} (28.4°C and 29.2°C, respectively). This was supported by daily estimates of LST (28.2°C), indicating the air was warmer than the irrigated turf grass during the warm season (see Table S1), in contrast to nonirrigated land covers in Phoenix (Song et al., 2017). We explore this seasonality further in Figures 2a and 2b by comparing the surface energy fluxes for the warm and cool seasons, shown as diurnal cycles of R_n , λET , H , and G (see Text S8 and Table S2). The majority of energy input (R_n) results as evaporative cooling (λET) in the warm and cool seasons (peak $\lambda ET/R_n$ of 0.70 and 0.47, respectively). Since H and G remain consistent across the two seasons (Figures 2a and 2b), reductions in R_n in the cool season or during cloudy days in the warm season lead to lower λET , an indication of an energy limitation in the turf grass. It is also noteworthy that λET is positive at night during the warm season (average of 59 W/m²), while H is negative (average of -43 W/m²), implying that air warms the turf grass during the night (Table S2). This nighttime behavior of λET and H , in particular during the warm season, are characteristic of the oasis effect (Warner, 2004). Only a small amount of energy is partitioned to deeper soil layers (low magnitude of G), consistent with the relation between T_{air} and T_{soil} .

The influence of irrigation extends to both the warm and cool seasons, such that surface energy fluxes are dominated by λET . Nevertheless, large variations are noted in the turf grass conditions, in particular in the relation between $NDVI$ and midday albedo (Figure 2b inset). In the cool season, rough areas decrease in $NDVI$ and increase in a , which reduces energy inputs via the effect of albedo on R_n . Seasonal differences are also apparent in CO_2 fluxes which are compared in Figures 2c and 2d as diurnal cycles of NEE and its two components: gross primary productivity (GPP) and ecosystem respiration (R_{eco} ; Text S9 and Table S4). Irrigated turf grass exhibits diurnal behavior that reflects photosynthetic processes, with daytime CO_2 uptake ($NEE < 0$) and nighttime CO_2 releases ($NEE > 0$). As expected, the warm season has higher GPP and R_{eco} , leading to higher CO_2 uptake, as turf grasses receive more irrigation and energy input, exhibit greater $NDVI$ and lower a , and grow in an environment of higher T_{air} and T_{soil} . Warm season CO_2 uptake during the day is considerably higher than reported values from irrigated turf grasses at other sites (Pahari et al., 2018), suggesting that biological processes are at maximum capacities, in particular for the warm season. In both seasons, a negligible impact of anthropogenic emissions, such as traffic, is noted on CO_2 fluxes, in contrast to other land covers in Phoenix (Pérez-Ruiz et al., 2020).

3.2. Oasis Effect

Due to its higher irrigation and energy input, we focus on identifying if there is an oasis effect during the warm season. Figures 3a and 3b present the daily variation of ET and two primary controlling factors, R_s and VPD , as obtained through a linear regression analysis (Text S4 and Table S3). Wind speed or direction were not significant controls, indicating that advected energy is omnidirectional. As expected, variations in ET reflect the seasonality of solar radiation and daily changes in R_s and VPD related to the North American monsoon (Vivoni et al., 2008). Daily ET from the EC method exhibited a strong relation with evapotranspiration estimates obtained as $K_c ET_o$ (Figure 3a inset), where K_c is a monthly varying crop coefficient (Brown et al., 2001; Text S5). This provided confidence in the use of the long-term ET_o estimates at the AZMET station (2003–2018) to determine days with an oasis effect (yellow circles in Figure 3). To generalize the method for other sites, we utilized T_{air} and RH as proxies for R_s and VPD . We identified the T_{air} and RH conditions during warm season days that exceeded the 90% quantile in $K_c ET_o$ in the 6,352-day record. This yielded a threshold of T_{air} that if exceeded at a particular RH indicates a day with the oasis effect, in a manner similar to the use of a heat index (Text S6 and Figure S4). Note that oasis days represent 36% of the warm season in Figure 3, including all of the EHW days in 2019, as compared to 21% in the long-term records, an indication of the exceptionally hot and dry conditions. Furthermore, the selection of oasis days generally results in high ET , R_s , and VPD , as compared to the long-term averages over 2003–2018 (Figures 3a and 3b).

Oasis days represent high-temperature and low-humidity settings leading to exceptionally large daily ET . Note that oasis days have average daily wind speeds and profile-averaged soil moisture values (1.62 m/s and $0.59 \text{ m}^3/\text{m}^3$) that are similar to nonoasis days (1.62 m/s and $0.55 \text{ m}^3/\text{m}^3$) during the warm season. Even the wind direction has a limited control on daily ET (Figure 3b inset), with days with winds from the west (240° to 300°) exhibiting similar values ($6.62 \pm 0.71 \text{ mm/day}$) to days from all other directions ($6.28 \pm 1.13 \text{ mm/day}$), despite having a residential area to the west. Given the high CO_2 sequestration potential of irrigated turf grasses, it is surprising that oasis days with high ET are also typically periods of CO_2 release to the atmosphere (average daily NEE of $3.78 \text{ g CO}_2 \text{ m}^{-2} \text{ day}^{-1}$; Figure 3c inset), due to higher nighttime R_{eco} as compared to daytime GPP (see Table S4). Nonoasis days are characterized by neutral CO_2 conditions (NEE near zero) such that a balance exists between plant productivity and respiration from soils, turf grasses, and lawn residues. Inherent water use efficiency ($IWUE$; Text S7) indicates that sustained plant productivity per unit of evaporative loss occurs throughout the warm season such that plants are at their maximum capacity and are not influenced by the advected energy during oasis days. These results are in contrast to studies in other climates showing that irrigated turf grasses primarily absorb CO_2 (Pahari et al., 2018). Overall, this points to the oasis effect having important outcomes for CO_2 releases from urban parks in desert cities.

Features of the oasis effect are shown in Figures 4a and 4b through a comparison of the diurnal cycles of R_n , λET , H , G , and NEE averaged over oasis ($n = 65$) and nonoasis ($n = 118$) days in the warm season (see Text S6 and Table S2). For reference, conditions during EHW days ($n = 26$) are also shown as dashed lines. As first reported by Spoken-Smith et al. (2000), the oasis effects in an urban park is characterized by a high daytime

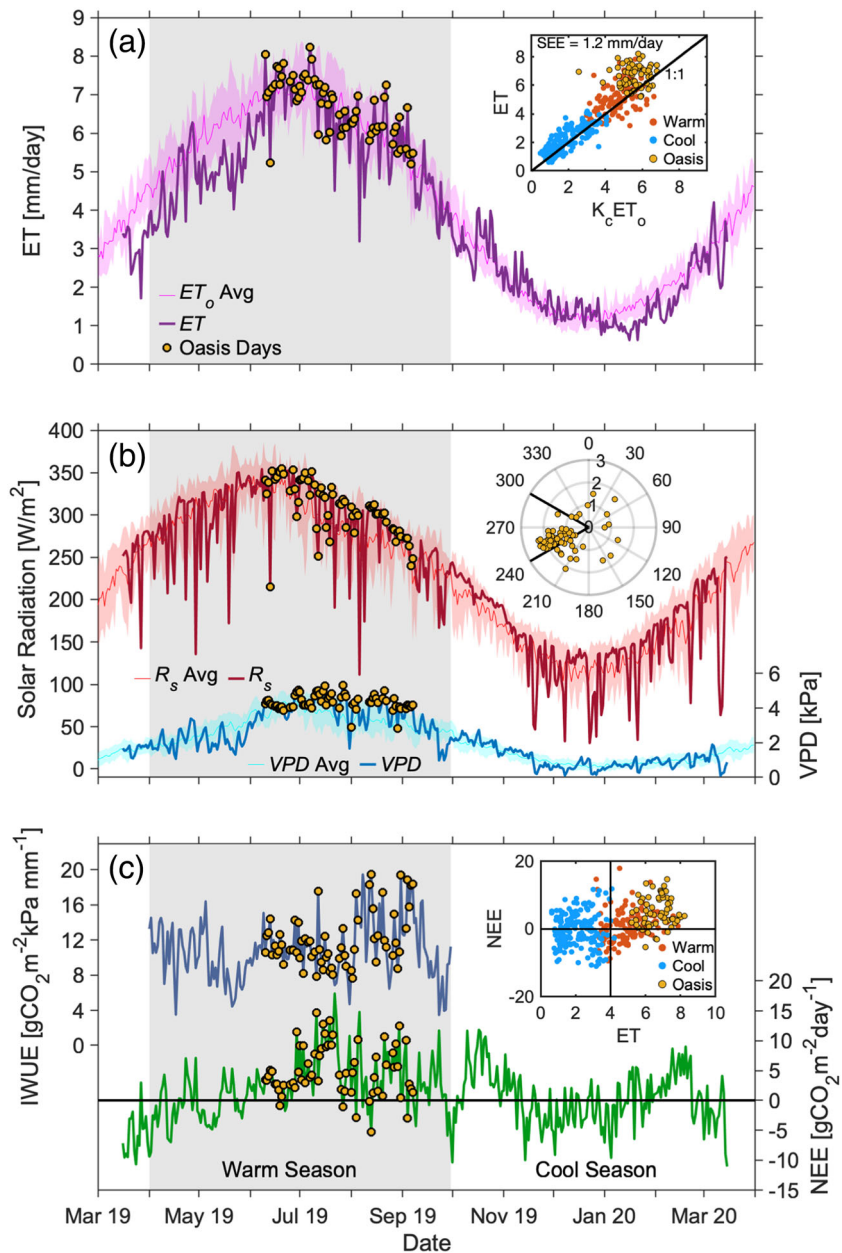


Figure 3. Daily variations in (a) ET and ET_o , (b) R_s and VPD , and (c) NEE and $IWUE$. Solid lines are study period observations, while thin lines with shading depict daily average values and ± 1 standard deviation over 2003–2018. Yellow circles represent oasis days. Inset in (a) compares daily ET with $K_c ET_o$ during the study period (see Text S5). Inset in (b) shows daily average wind speed (m/s) and direction ($^\circ$ from North) for oasis days. Inset in (c) is the relation between daily ET and NEE in four quadrants with thresholds of $NEE = 0 \text{ g CO}_2 \text{ m}^{-2} \text{ day}^{-1}$ and $ET = 4 \text{ mm day}^{-1}$.

and nighttime λET . During oasis days, the ratio of peak $\lambda ET/R_n$ rises from 0.62 to 0.80 (28% higher), while the peak ratio of H/R_n is reduced from 0.18 to 0.10 (41% lower). Another distinguishing feature is the late afternoon period when λET can exceed R_n as additional energy is input via a negative H (average H of -31 W/m^2 over 5:00 to 9:00 p.m.). Energy input during oasis days is likely affected by advection from surrounding urban areas in all directions that are hotter and drier, leading to a higher R_n , a more negative H , and an increase in λET (average peak differences of $+56$, -40 , and $+142 \text{ W/m}^2$, respectively). This is consistent with Spoken-Smith et al. (2000), who first performed measurements in an urban park and its surroundings. The authors also indicated that separately accounting for advected energy is not feasible

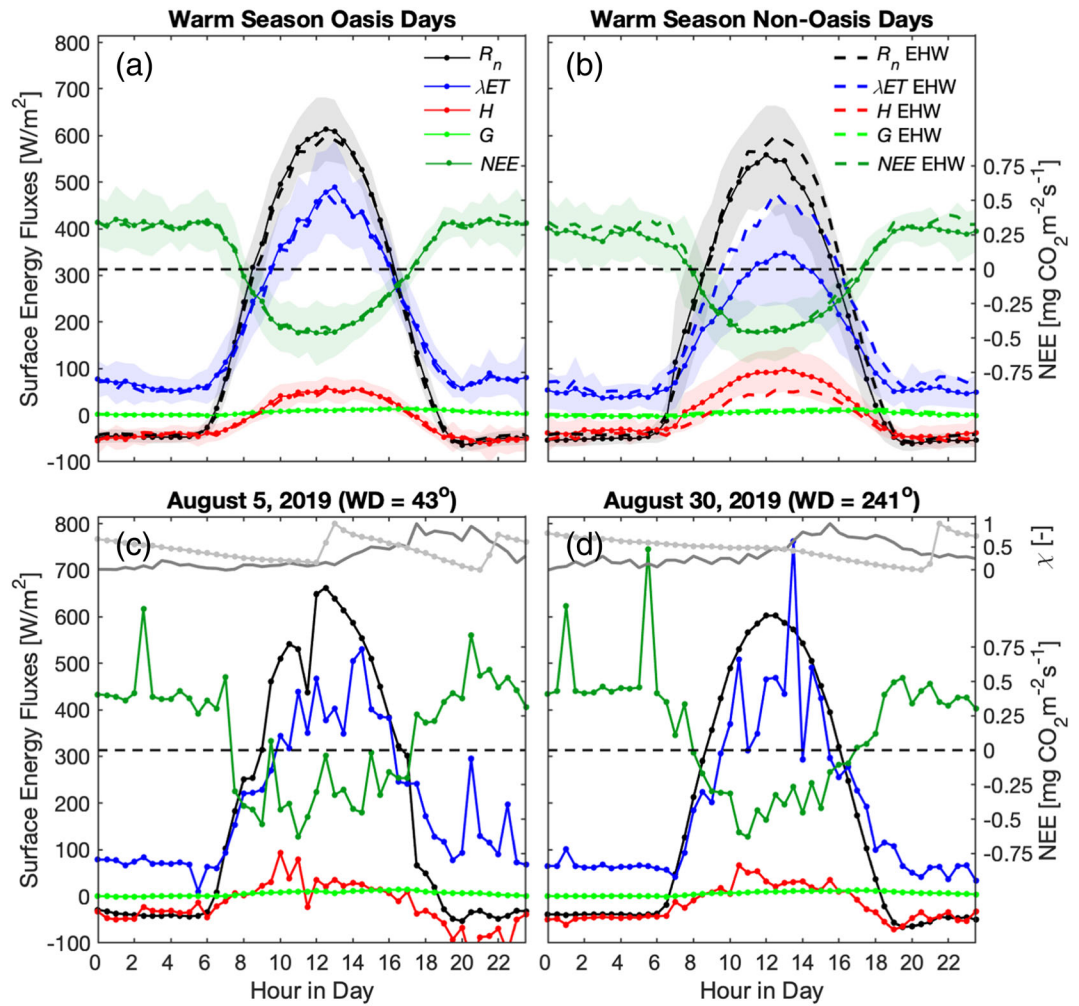


Figure 4. Diurnal cycles of surface energy fluxes and *NEE* during warm season for (a) oasis days and (b) all other days (labeled nonoasis). Symbols indicate average values for each 30-min interval in each subset, while envelopes depict the ± 1 standard deviation. Dashed lines represent excessive heat warning (EHW) days in both (a) and (b) as a comparison. (c, d) Diurnal cycles for two oasis days (5 and 30 August 2019) with different wind directions (*WD*, ° from North), along with shallow soil moisture (gray dots) and maximum wind speed (gray line) shown as normalized quantities (χ , Text S10).

during oasis conditions since it has a direct impact on all other fluxes. Interestingly, only a minor effect is noted on *NEE* during oasis days, with a small increase in *NEE* observed at night due to an increase in R_{eco} under the warmer temperatures of oasis days. This suggests that turf grass transpiration does not adjust to the additional energy input due to the oasis effect as plants are at their maximum capacity, as confirmed by no daytime change in *NEE* and *GPP*. As a result, an abiotic process should be responsible for the higher daytime λET . Chow et al. (2014) also noted some of the oasis effect features within an urban area of Phoenix but did not attribute the observed increase in λET to specific evaporative processes.

An inspection of representative oasis days yields insights on the factors influencing the high evaporative loss. Figures 4c and 4d show the diurnal cycles of R_n , λET , *H*, *G*, and *NEE* for two oasis days (5 and 30 August 2019) that were also identified as EHW days. These days recorded no rainfall and capture differing wind directions (*WD* of 43 and 241° from North) that sample the variability in contributions from neighboring areas during the warm season. To provide context, normalized soil moisture in the shallow 5 cm sensor and maximum wind speed are shown (see Text S10). Note the late afternoon periods when is λET greater than R_n due to the energy input from *H*. In contrast to this consistent feature of the oasis effect (Warner, 2004), some oasis days also exhibit large increases in λET during the midafternoon as shown in Figure 4d. These are attributed

to large increases in wind speed, in particular when wind directions are from the west (240 to 300°), and are coincident with midafternoon decreases in H , but no discernable changes in NEE . We attribute these short-lived increases to a more localized impact of wind gusts from the residential area to the west. Interesting behavior occurs in response to irrigation as depicted through a delayed rise in the shallow soil moisture. At night, irrigation via sprinkler application promotes a short pulse in λET that is associated with an increased CO_2 release (higher R_{eco}). This suggests that nighttime irrigation during oasis days is the primary reason for turf grass to be a net CO_2 source. Note that nighttime λET and R_{eco} account for 36% and 52% of daily values during oasis conditions (Tables S2 and S4). Furthermore, increased λET is not linked to plant productivity such that additional energy is partitioned through abiotic mechanisms such as evaporation from direct sprinkler water, intercepted water on turf grasses, and soils that are wet down to 30 cm.

4. Concluding Remarks

We identify that the oasis effect is a persistent warm season feature of an irrigated turf grass which is closely linked to periods of high air temperature and low humidity associated with EHWs. While previously thought to occur, direct evidence has not been documented at the level of detail provided here. The large distance of the site to the golf course edge suggests that advected energy is input from local surroundings in all directions rather than being an edge effect (Sproken-Smith et al., 2000). Nonetheless, certain oasis days have short periods with high winds from a neighborhood to the west that briefly elevate latent heat flux. It is important to note that the oasis effect has impacts on both daytime and nighttime conditions (see Text S11). During short periods at midday and late afternoons, latent heat flux can exceed net radiation since advected energy and irrigated conditions lead to downward sensible heat flux. At night, latent heat flux increases in response to higher amounts of advected energy and often has short pulses occurring after irrigation. These features are muted or absent from days that do not meet the oasis conditions based on daily air temperature and RH data.

A summary of the CO_2 budget offers novel insights on the oasis effect (see Text S11). Daytime plant productivity is unaffected by advected energy, indicating that latent heat flux increases are not related to higher turf grass transpiration. This contradicts van Bavel et al. (1963) who attributed higher evaporative losses under advected energy to an increase in grass transpiration. Instead, latent heat fluxes are higher due to the increased evaporation from soils and direct evaporation of irrigation and from intercepted water on the turf itself. Interestingly, nighttime evaporative losses occur under conditions of CO_2 release. While evaporative losses during short pulses are associated to sprinkler water application, more persistent latent heat fluxes are linked to soil evaporation and possibly to nighttime transpiration identified to occur in warm season grasses (O'Keefe & Nippert, 2018). Additional CO_2 releases during the oasis effect are likely due to higher soil and turf grass respiration upon soil wetting from irrigation.

The existence of a warm season oasis effect in arid and semiarid regions has important implications for the urban heat island, CO_2 emissions, and heat-related health hazards. Our findings suggest that the oasis effect can be identified for other parks using readily available data. When EHWs are issued, for instance, the oasis effect provides enhanced evaporative cooling in irrigated areas and their downwind locations. This enhances the suitability of urban parks as a heat mitigation strategy (Zhang et al., 2017). Furthermore, the oasis effect is anticipated to become more prevalent during the warm season under the combined effects of urbanization and climate change which are increasing EHWs.

Data Availability Statement

Data sets for the study period are available at Zenodo (Kindler et al., 2020).

Acknowledgments

We thank the City of Phoenix Parks and Recreation Department for their support in obtaining site permits and data sets. Planet imagery was made available through the Planet Incubator Program.

References

- Baldocchi, D., Falge, E., Gu, L., Olson, R., Hollinger, D., Running, S., et al. (2001). FLUXNET: A new tool to study the temporal and spatial variability of ecosystem-scale carbon dioxide, water vapor, and energy flux densities. *Bulletin of the American Meteorological Society*, *82*(11), 2415–2434.
- Brown, P. W., Mancino, C. F., Young, M. H., Thompson, T. L., Wierenga, P. J., & Kopec, D. M. (2001). Penman Monteith crop coefficients for use with desert turf systems. *Crop Science*, *41*, 1197–1206.
- Brown, R. D., Vanos, J., Kenny, N., & Lenzholzer, S. (2015). Designing urban parks that ameliorate the effects of climate change. *Landscape and Urban Planning*, *138*, 118–131.
- Buyantuyev, A., & Wu, J. (2010). Urban heat islands and landscape heterogeneity: Linking spatiotemporal variations in surface temperatures to land-cover and socioeconomic patterns. *Landscape Ecology*, *25*(1), 17–33.

- Chen, J., Jönsson, P., Tamura, M., Gu, Z., Matsushita, B., & Eklundh, L. (2004). A simple method for reconstructing a high-quality NDVI time-series data set based on the Savitzky-Golay filter. *Remote Sensing of Environment*, *91*(3–4), 332–344.
- Chow, W. T. L., Brennan, D., & Brazel, A. J. (2012). Urban heat island research in Phoenix, Arizona: Theoretical contributions and policy applications. *Bulletin of the American Meteorological Society*, *93*(4), 517–530.
- Chow, W. T. L., Pope, R. L., Martin, C. A., & Brazel, A. J. (2011). Observing and modeling the nocturnal park cool island of an arid city: Horizontal and vertical impacts. *Theoretical and Applied Climatology*, *103*(2), 197–211.
- Chow, W. T. L., Volo, T. J., Vivoni, E. R., Jenerette, G. D., & Ruddell, B. L. (2014). Seasonal dynamics of a suburban energy balance in Phoenix, Arizona. *International Journal of Climatology*, *34*(15), 3863–3880.
- Colter, K. R., Middel, A. C., & Martin, C. A. (2019). Effects of natural and artificial shade on human thermal comfort in residential neighborhood parks of Phoenix, Arizona, USA. *Urban Forestry & Urban Greening*, *44*, 126429. <https://doi.org/10.1016/j.ufug.2019.126429>
- Cook, W. M., & Faeth, S. H. (2006). Irrigation and land use drive ground arthropod community patterns in an urban desert. *Environmental Entomology*, *35*(6), 1532–1540.
- Day, T. A., Gober, P., Xiong, F. S., & Wentz, E. A. (2002). Temporal patterns in near-surface CO₂ concentrations over contrasting vegetation types in the Phoenix metropolitan area. *Agricultural and Forest Meteorology*, *110*, 229–245.
- Gober, P., Brazel, A., Quay, R., Myint, S., Grossman-Clarke, S., Miller, A., & Rossi, S. (2010). Using watered landscapes to manipulate urban heat island effects: How much water will it take to cool Phoenix? *Journal of the American Planning Association*, *76*(1), 109–121.
- Harlan, S. L., Brazel, A. J., Prashad, L., Stefanov, W. L., & Larsen, L. (2006). Neighborhood microclimates and vulnerability to heat stress. *Social Science & Medicine*, *63*(11), 2847–2863. <https://doi.org/10.1016/j.socscimed.2006.07.030>
- Houborg, R., & McCabe, M. F. (2018). Daily retrieval of NDVI and LAI at 3 m resolution via the fusion of CubeSat, Landsat, and MODIS data. *Remote Sensing*, *10*(6), 890. <https://doi.org/10.3390/rs10060890>
- Kindler, M., Perez-Ruiz, E. R., Wang, Z., & Vivoni, E. R. (2020). Water, energy and carbon fluxes and ancillary meteorological and remote sensing measurements at Encanto Golf Course, Phoenix, Arizona during 2019–2020 <http://doi.org/10.5281/zenodo.3872381>
- Kljun, N., Calanca, P., Rotach, M. W., & Schmid, H. P. (2015). A simple two-dimensional parameterisation for Flux Footprint Prediction (FFP). *Geoscientific Model Development*, *8*(11), 3695–3713.
- Ko, A., Mascaro, G., & Vivoni, E. R. (2016). Irrigation impacts on scaling properties of soil moisture and the calibration of a multifractal downscaling algorithm. *IEEE Transactions on Geoscience and Remote Sensing*, *54*(6), 3128–3142.
- Koerner, B., & Klopatek, J. (2002). Anthropogenic and natural CO₂ emission sources in an arid urban environment. *Environmental Pollution*, *116*, S45–S51.
- Larson, E. K., & Perrings, C. (2013). The value of water-related amenities in an arid city: The case of the Phoenix metropolitan area. *Landscape and Urban Planning*, *109*, 45–55.
- Li, X., Myint, S. W., Zhang, Y., Galletti, C., Zhang, X., & Turner, B. L. (2014). Object-based land-cover classification for metropolitan Phoenix, Arizona, using aerial photography. *International Journal of Applied Earth Observation and Geoinformation*, *33*, 321–330.
- Martin, M., Ghent, D., Pires, A., Göttsche, F.-M., Cermak, J., & Remedios, J. J. (2019). Comprehensive in situ validation of five satellite land surface temperature data sets over multiple stations and years. *Remote Sensing*, *11*(5), 479. <https://doi.org/10.3390/rs11050479>
- Mascaro, G. (2018). On the distributions of annual and seasonal daily rainfall extremes in central Arizona and their spatial variability. *Journal of Hydrology*, *559*, 266–281.
- Motazedian, A., Coutts, A. M., & Tapper, N. J. (2020). The microclimatic interaction of a small urban park in central Melbourne with its surrounding urban environment during heat events. *Urban Forestry & Urban Greening*, *52*, 126688.
- Myint, S. W., Wentz, E. A., Brazel, A. J., & Quattrochi, D. A. (2013). The impact of distinct anthropogenic and vegetation features on urban warming. *Landscape Ecology*, *28*(5), 959–978.
- NWS, National Weather Service (2019). Monsoon 2019 Review for the Southwest U.S. Available at: <https://www.weather.gov/psr/SouthwestMonsoon2019Review>
- O’Keefe, K., & Nippert, J. B. (2018). Drivers of nocturnal water flux in a tall grass prairie. *Functional Ecology*, *32*, 1155–1167.
- Pahari, R., Leclerc, M. Y., Zhang, G., Nahrawi, H., & Raymer, P. (2018). Carbon dynamics of a warm season turfgrass using the eddy-covariance technique. *Agriculture, Ecosystems and Environment*, *251*, 11–25.
- Park, S. (2017). A preliminary study on connectivity and perceived values of community green spaces. *Sustainability*, *9*(5), 692. <https://doi.org/10.3390/su9050692>
- Pérez-Ruiz, E. R., Vivoni, E. R., & Templeton, N. P. (2020). Urban land cover type determines the sensitivity of carbon dioxide fluxes to precipitation in Phoenix, Arizona. *PLoS ONE*, *15*(2), e0228537. <https://doi.org/10.1371/journal.pone.0228537>
- Planet Labs (2017). Planet application program interface. In *Space for life on Earth*. San Francisco, CA: Planet Labs. Retrieved from <https://api.planet.com>
- Shepherd, J. M. (2006). Evidence of urban-induced precipitation variability in arid climate regimes. *Journal of Arid Environments*, *67*(4), 607–628.
- Soil Survey Staff, Natural Resources Conservation Service, United States Department of Agriculture. (2020). Web soil survey. Available online at the following link: <http://websoilsurvey.sc.egov.usda.gov/>. Accessed 03/31/2020.
- Song, J., & Wang, Z.-H. (2015). Impacts of mesic and xeric urban vegetation on outdoor thermal comfort and microclimate in Phoenix, AZ. *Building and Environment*, *94*(2), 558–568.
- Song, J. Y., Wang, Z. H., Myint, S. W., & Wang, C. (2017). The hysteresis effect on surface-air temperature relationship and its implication to urban planning: An examination in Phoenix, Arizona, USA. *Landscape and Urban Planning*, *167*, 198–211.
- Sproken-Smith, R. A., Oke, T. R., & Lowry, W. P. (2000). Advection and the surface energy balance across an irrigated urban park. *International Journal of Climatology*, *20*, 1033–1047.
- Templeton, N. P., Vivoni, E. R., Wang, Z.-H., & Schreiner-McGraw, A. P. (2018). Quantifying water and energy fluxes over different urban land covers in Phoenix, Arizona. *Journal of Geophysical Research: Atmospheres*, *123*, 2111–2128. <https://doi.org/10.1002/2017JD027845>
- van Bavel, C. H. M., Fritschen, L. J., & Reeves, W. E. (1963). Transpiration by Sudan grass as an externally controlled process. *Science*, *141*(3577), 269–270. <https://doi.org/10.1126/science.141.3577.269-a>
- Vivoni, E. R., Moreno, H. A., Mascaro, G., Rodriguez, J. C., Watts, C. J., Garatuza-Payan, J., & Scott, R. L. (2008). Observed relation between evapotranspiration and soil moisture in the North American monsoon region. *Geophysical Research Letters*, *35*, L22403. <https://doi.org/10.1029/2008GL036001>
- Warner, T. T. (2004). *Desert Meteorology* (p. 595). Cambridge, UK: Cambridge University Press.
- Wilson, K., Goldstein, A., Falge, E., Aubinet, M., Baldocchi, D., Berbigier, P., et al. (2002). Energy balance closure at FLUXNET sites. *Agricultural and Forest Meteorology*, *113*(1–4), 223–243.

- Yabiku, S. T., Casagrande, D. G., & Farley-Metzger, E. (2008). Preferences for landscape choice in a Southwestern desert city. *Environment and Behavior*, *40*(3), 382–400.
- Zhang, Y., Murray, A. T., & Turner, B. L. (2017). Optimizing green space locations to reduce daytime and nighttime urban heat island effects in Phoenix, Arizona. *Landscape and Urban Planning*, *165*, 162–171.

References From the Supporting Information

- Beer, C., Ciais, P., Reichstein, M., Baldocchi, D., Law, B. E., Papale, D., et al. (2009). Temporal and among-site variability of inherent water use efficiency at the ecosystem level. *Global Biogeochemical Cycles*, *23*, GB2018. <https://doi.org/10.1029/2008GB003233>
- Brown, P. W. (2005). *Standardized reference evapotranspiration: A new procedure for estimating reference evapotranspiration in Arizona, AZ1324* (p. 12). Tucson, AZ: The University of Arizona.
- Brown, P. W., & Kopec, D. (2014). *Converting reference evapotranspiration into turf water use, AZ1195* (p. 5). Tucson, AZ: The University of Arizona.
- Foken, T. (2006). 50 Years of the Monin-Obukhov similarity theory. *Boundary-Layer Meteorology*, *119*, 431–447.
- Jensen, M. E., Burman, R. D., & Allen, R. G. (1990). Evapotranspiration and irrigation water requirements. ASCE Manuals and Reports on Engineering (Practice No. 70, p. 360). New York, N.Y.
- Massman, W. J. (2001). Reply to comment by Rannik on: A simple method for estimating frequency response corrections for eddy covariance systems. *Agricultural and Forest Meteorology*, *107*, 247–251.
- Moncrieff, J. B., Clement, R., Finnigan, J., & Meyers, T. (2004). Averaging, detrending, and filtering of eddy covariance time series. In *Handbook of Micrometeorology* (pp. 7–31). Dordrecht: Springer.
- Moncrieff, J. B., Massheder, J. M., De Bruin, H., Elbers, J., Friborg, T., Heusinkveld, B., et al. (1997). A system to measure surface fluxes of momentum, sensible heat, water vapour and carbon dioxide. *Journal of Hydrology*, *188*, 589–611.
- Paw U, K. T., Baldocchi, D. D., Meyers, T. P., & Wilson, K. B. (2000). Correction of eddy-covariance measurements incorporating both advective effects and density fluxes. *Boundary-Layer Meteorology*, *97*, 487–511.
- Rothfus, L.P. (1990). The heat index “equation”. NWS Southern Region (Tech. Attachment SR-9023, p. 2) Available online at http://www.weather.gov/media/ffc/ta_htindx.PDF
- Schmid, H. P., Grimmond, C. S. B., Cropley, F., Offerle, B., & Su, H. B. (2000). Measurements of CO₂ and energy fluxes over a mixed hardwood forest in the mid-western United States. *Agricultural and Forest Meteorology*, *103*(4), 357–374.
- Webb, E. K., Pearman, G. I., & Leuning, R. (1980). Correction of flux measurements for density effects due to heat and water vapor transfer. *Quarterly Journal of the Royal Meteorological Society*, *106*, 85–106.
- Wilczak, J. M., Oncley, S. P., & Stage, S. A. (2001). Sonic anemometer tilt correction algorithms. *Boundary-Layer Meteorology*, *99*, 127–150.
- Wutzler, T., Lucas-Moffat, A., Migliavacca, M., Knauer, J., Sickel, K., Šigut, L., et al. (2018). Basic and extensible post-processing of eddy covariance flux data with REddyProc. *Biogeosciences*, *15*(16), 5015–5030.